Controlled NTM Healing by Fueling Pellets and its Impact on Electron Cyclotron Current Drive Requirements for Complete NTM Stabilization

L. Bardóczi,[1,2,a)] M. J. Choi,[3] A. Bañón Navarro,[4] D. Shiraki,[5] R. J. La Haye,[1] S. H. Park,[3] M. Knölker,[6] T. E. Evans,[1] G. R. McKee,[7] M. Woo,[3] B. H. Park,[3] and F. Jenko[4,8]

[1)] *General Atomics, P. O. Box 85608, San Diego, California 92186-5608, USA*
[2)] *Oak Ridge Associated Universities, Oak Ridge, Tennessee 37831, USA*
[3)] *National Fusion Research Institute, Daejeon 34133, Republic of Korea*
[4)] *Max-Planck-Institut für Plasmaphysik, Garching, Germany*
[5)] *Oak Ridge National Laboratory, Oak Ridge, Tennessee 37831, USA*
[6)] *Princeton Plasma Physics Laboratory, Princeton University, Princeton, New Jersey 08543, USA*
[7)] *University of Wisconsin-Madison, Madison, Wisconsin 53706, USA*
[8)] *University of Texas at Austin, Austin, Texas 78712, USA*

(Dated: 9 September 2019)

Controlled partial stabilization of core $m/n = 2/1$ Neoclassical Tearing Modes (NTMs) by fueling deuterium pellets is reported in DIII-D and KSTAR H-mode plasmas (m/n are the poloidal/toroidal mode numbers). Analyses of DIII-D data exploring possible physics origins show that an explanation is offered by NTM-turbulence multi-scale interaction, triggered by a sudden increase of local gradients near $q = 2$ caused by the pellet. Pellet injection from the high-field side allows deep fueling which reaches the island region. In turn, low-k turbulent density fluctuations ($\tilde{n}$) increase by 30% in the island region. This $\tilde{n}$ can drive transport across the island separatrices, reducing the pressure flat spot at the O-point and diminishing the NTM drive. The Mirnov probe array detects the reduction of the 2/1 magnetic amplitude by up to 20%. Causality between elevated gradients outside of the island, turbulence spreading into the island and reduced NTM drive is qualitatively supported by non-linear gyrokinetic turbulence simulations. These show increased penetration of ion-scale $\tilde{n}$ from the background plasma to the O-point region when the background gradient is increased. This interaction has potentially far reaching consequences as it can lead to a reduction of the required electron cyclotron current density (j_{ECCD}) for NTM suppression by 70%, as predicted by the modified Rutherford equation. This beneficial effect of fueling pellets can be important as j_{ECCD} is the anticipated active NTM control technique for the International Thermonuclear Experimental Reactor (ITER), but its efficiency will be lowered by third harmonic absorption in Pre-Fusion Power Operation-1 (PFPO-1) at half magnetic field.

I. INTRODUCTION

The $m/n = 2/1$ Neoclassical Tearing Mode (NTM) is a major impediment in the development of operational scenarios of present and future tokamaks, as it degrades plasma confinement and, if large enough, often locks to the wall, slows down the plasma rotation and leads to plasma termination[1,2] (m/n are the poloidal/toroidal mode numbers). NTMs are destabilized by a helical bootstrap current perturbation (δj_{BS}) arising due to 'missing' pressure gradient (∇p) at the magnetic island O-point[3–5]. NTM stabilization has been achieved by electron cyclotron current drive (ECCD) in various H-mode scenarios by replacing δj_{BS} at the mode rational surface[6–9]. This control method is the leading candidate for active NTM stabilization in ITER burning plasmas. However, in ITER Pre-Fusion Power Operation-1 (PFPO-1), the high electron density (n_e) at low magnetic field (B) imposes a major concern for NTM stabilization via ECCD due to parasitic 3rd harmonic absorption in the edge which lowers ECCD efficiency in the core[10]. Therefore, the avoidance of locked mode–induced disruptions in ITER start up operations would benefit from an active NTM control method that does not rely on high gyrotron power. Such a method may also improve the net electricity output of future reactors and/or could free up gyrotrons for heating and current drive elsewhere in the plasma.

A solution is offered by restoring ∇p at the island O-point which can be accomplished in practice by fueling pellets. Experimentally observed T_e structures of magnetic islands are well described[11–14] by a simple anisotropic diffusion model[15] ($\chi_\perp \nabla_\perp^2 T_e + \chi_\parallel \nabla_\parallel^2 T_e = 0$, where $\chi_\parallel$ is the parallel electron thermal diffusivity), where T_e is flat if $\chi_\perp = 0$ at the O-point, but finite $\chi_\perp$ results in a boundary layer $L_\chi \propto \chi_\perp^{1/4}$ which decreases the δj_{BS} drive of the NTM. Inside the island, $\chi_\perp$ is reduced to neoclassical level[12–14], in accord with local reduction of ion temperature gradient (ITG) and trapped electron mode (TEM) scale turbulence[16–18]. Under these conditions $L_\chi \approx 1.2$ cm[14], but in principle $L_\chi \approx 4$ cm is possible by restoring $\tilde{n}$ inside the island. This is viable through turbulence spreading[19], allowing $\tilde{n}$ to propagate radially[20] into the linearly stable O-point region, delocalizing the relation between $\tilde{n}$ intensity (and $\chi_\perp$)

a)Electronic mail: bardoczil@fusion.gat.com

and ∇T_e, as reported in recent magnetic island experiments in DIII-D[21]. As gradients are turbulence drives, it is expected that a surge in gradients outside the island (caused by the pellet) can reduce the j_{BS} drive of the NTM through $\tilde{n}$ spreading.

Formation of magnetic islands due to pellets and triggered growth of pre-existing small magnetic islands by pellets have been observed[22–26]. Pellets have been also utilized to study the perpendicular particle transport in the O-point region of islands[27,28]. NTM suppression by fueling pellets, however, has not been reported before.

In this paper we present controlled partial stabilization of NTMs by fueling pellets for the first time in DIII-D[29] and KSTAR[30] H-mode discharges, investigate possible physics origins of this behavior and discuss consequences on ECCD requirements for complete NTM stabilization. In these experiments, pellet injection from the high-field side allows density (δn_e) and temperature perturbations (δT) to propagate to the NTM rational surface in a few milliseconds, due to favorable polarization drift of the ablated pellet material[31]. DIII-D data shows that these enhance local gradients in the island region, which are turbulence drives, and concomitant low-k $\tilde{n}$ levels in the expected range of the Micro Tearing Mode and Trapped Electron Mode instabilities. When the pellet–driven perturbations reach the island region, the islands shrink by maximum 20% and then recover in about 40 ms in DIII-D. In KSTAR, the islands shrink by maximum 30% and then recover in about 80 ms. Analyses suggest that classical stability can not change in this time scale and changes in the resistivity or the rotation are not the underlying causes of this behavior. Reduced j_{BS} drive due to enhanced cross-field transport inside the island offers a quantitative explanation of the reported phenomenon.

Complementing the experimental data, non-linear GENE[32] gyrokinetic simulations with magnetic islands were employed to investigate causality between elevated gradients outside of the island, turbulence spreading into the island and reduced δj_{BS} at the O-point region. These show that increased gradients outside of the island increase the $\tilde{n}$ radial correlation and $\tilde{n}$ spreading into the O-point region. The layer of finite gradients inside the island (L_χ) increases with $\tilde{n}$, which in turn reduces δj_{BS}. Interestingly, the modified Rutherford equation (MRE) predicts that a transport enhancement inside the island can reduce the required j_{ECCD} for complete NTM stabilization by 70%.

The paper is structured as follows. DIII-D experimental set-up and observations are described in Section II and Section III, respectively, with KSTAR data included in Subsection III D. Physics origins of the reported behavior are investigated in Section IV. Evolution of DIII-D plasma profiles and low-k $\tilde{n}$ are discussed in Section V, gyrokinetic simulations in Section VI and implications on ECCD requirements in Section VII. Section VIII summarizes the study.

II. EXPERIMENTAL OVERVIEW

The response of naturally occurring and rotating 2/1 NTMs to fueling deuterium pellets was studied in reproducible, stationary hybrid DIII-D H-mode plasma conditions. The plasma shape was biased up double null [Fig. 1 (a)], the major radius of the magnetic axis was R_o=173 cm, minor radius was a=60 cm, elongation was $\kappa = 1.83$. A steady plasma current of 1.4 MA was maintained, in the stationary state the neutral beam power was 4.65 MW [Fig. 1 (b)], the line averaged density was $5.5 \times 10^{19} m^{-3}$ [FIG 1 (c)] (interferometry[33]), the toroidal magnetic field was $B_T = -1.86$ T. The square root of the normalized toroidal flux surface label of the $q = 2$ rational surface was $\rho \approx 0.68$. At this location the electron temperature (T_e, Thomson scattering[34]) and ion temperature (T_i, Charge Exchange Recombination, CER[35]) were both approximately 1.5 keV [FIG 1 (d)]. The normalized plasma beta was 1.39 ($\beta_N = \beta\, a B_T / I_P$) [FIG 1 (e)]. The $n = 1$ magnetic amplitude (Mirnov) started growing at about 2000 ms and saturated around 18 Gauss [FIG 1 (f)]. The frequency of this mode is 15 kHz initially and 5 kHz in the stationary state and the poloidal mode number is $m = 2$. The full width of the magnetic islands in the outboard mid-plane was $W \approx 8$ cm at $q = 2$ as seen in ECE[36] and ECEI[37] data in the discharges without pellets. In the discharges with pellets T_e measurements are possible only with the slower Thomson scattering system as ECE is cut off due to the higher density. In addition, all of these plasmas exhibit an $m/n = 3/2$ mode at $q = 1.5$, which is responsible for maintaining $q_{min} > 1$ which keeps the core sawtooth free.

During the flat top phase of the discharge when the NTM amplitude has saturated, 1.8 mm deuterium pellets are injected from the high-field side at 45 degree poloidal angle [Fig. 1 (a)], at a rate of 10 Hz, starting at $t = 2318$ ms. With typical velocities of 150 to 200 m/s, the pellets are ablated within 15 cm of the plasma edge, but the resulting δn_e and δT propagate to the island region in a few milliseconds due to polarization drifts[31]. Along the pellet trajectory, the $q = 2$ surface is 31 cm from the last closed flux surface. A clear signature of the pellet is a surge in n_e [Fig. 1 (c)]. Concomitant drops of T_e and T_i leas to no or nearly no change in β [Fig. 1 (e)]. These events are accompanied by a drop of the 2/1 amplitude by typically about 20% [Fig. 1 (f)], which is evidence that core fueling pellets have stabilizing effect on pre-existing saturated 2/1 NTMs.

III. RESPONSE OF 2/1 NTMS TO PELLETS

Several of the utilized pellets broke into two or more pieces before reaching the vacuum chamber, which resulted in the variation of the induced δT and δn. Fig. 1 shows the evolution of the line integrated n_e (g), T_e and T_i outside of the island on the low field side (h), 2/1 NTM magnetic amplitude (i), the raw Mirnov signal (j)

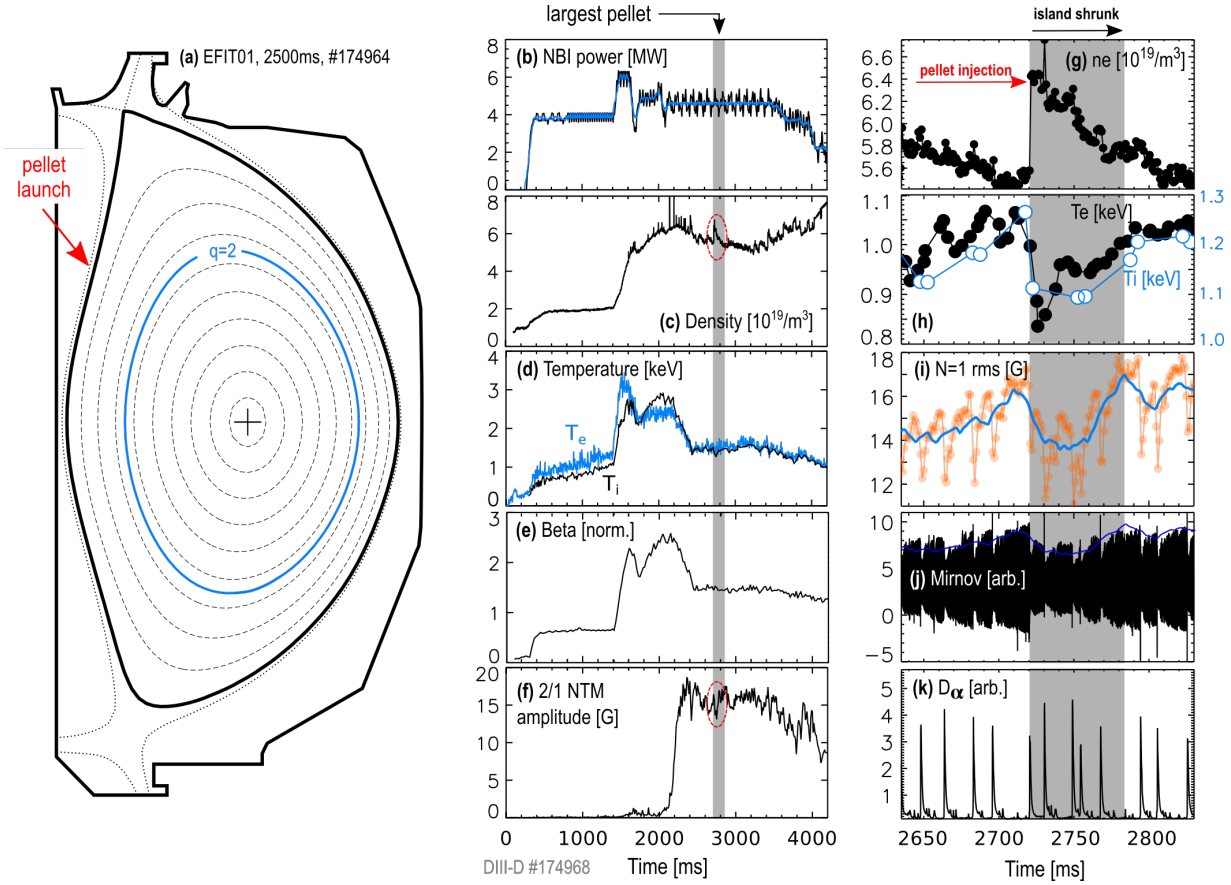

FIG. 1: (a) Equilibrium reconstruction with pellet launch geometry. (b) Neutral beam power, (c) density (Thomson), (d) electron (T_e, Thomson) and ion temperature (T_i, CER) inside the radial region of the 2/1 island, (e) normalized plasma beta, (f) n=1 magnetic RMS (Mirnov). Time trace of (g) n_e, (h) T_e and T_i, (i) $n = 1$ magnetic amplitude (thin orange line with circles: raw signal with 1 ms resolution, thick blue line: raw signal smoothed with 20 ms time constant), (j) raw poloidal magnetic field fluctuation at the tokamak wall (Mirnov) and (k) Divertor D_α signal during the injection of the largest pellet of the discharge.

and the divertor D_α signal (k) during the injection of the largest pellet that reached the plasma in one piece. The surge of n_e is accompanied by a drop in the local T_e and T_i. Notice that the recovery of T_e and T_i takes about 60 ms, which is tracked by the $n = 1$ NTM amplitude. Both natural ELMs and the pellets can cause the island to shrink. Additionally, the pellets trigger ELMs, which also interact with the island. These are discussed in Subsections III A-III C, where phase-locking analysis of the $n = 1$ magnetic amplitude is employed to isolate the effect of ELMs and pellets on the 2/1 NTM.

A. Effect of natural ELMs on NTMs

On top of the pellet-caused perturbation, faster drops of the NTM amplitude are also observed in Fig. 1 (i), which consistently align with Edge Localized Modes (ELMs) in the D_α signal in Fig. 1 (k). These drops are not the ELM magnetic component, but reflect the shrinking and recovery of the 2/1 islands in about 10 ms after ELMs[38,39]. This evolution is also seen directly in the raw Mirnov signal in Fig. 1 (j). Additionally to the island response, some ELMs cause a sharp positive or negative spike in the Mirnov signal (but not in the slower $n = 1$ signal), which lasts only for about 0.1 ms. These spikes are interpreted as the magnetic component of ELMs, not a rapid change in the n=1 NTM amplitude.

The $T_e(t, R)$ contour phase-locked to ELMs in the lower density shots in Fig. 2 (a) shows that the ELM–induced "cold-pulse" in the edge plasma propagates to the island on sub-millisecond time-scale. In sync, the $m/n = 2/1$ island heals and then recovers in less than 10 ms. [Fig. 2 (b)]. The maximum perturbation of the "cold-pulse" reaches the island region about 5 ms after the ELM. This data is taken at lower density ($n_e \approx 3.2 \times 10^{19} m^{-3}$; without pellets), where the second harmonic ECE is not cut off, hence local measurements of T_e are possible. On average, T_e drops at $q = 2$ by 5% and the $n = 1$ amplitude drops by 20%. The island structure can be monitored by phase-locking local measurements of T_e to the island rotation frequency[14,40,41], which transforms the $T_e(R, t)$ data (from the lab frame) to $T_e(R, \xi)$ (to the island frame). Here $\xi = m\theta - n\phi$ is the helical phase of the island, θ and ϕ are the poloidal and

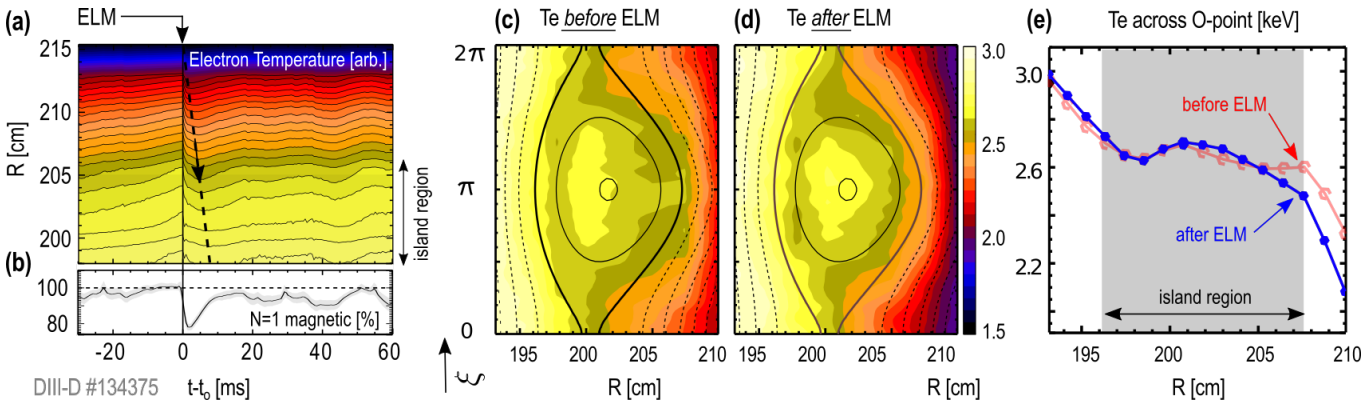

FIG. 2: Effect of natural ELMs on the structure $m/n = 2/1$ NTM magnetic islands: (a) inward propagating T_e "cold"-pulse in ECE data phase-locked to ELMs. (b) $n = 1$ magnetic signal shows island shrinking after ELMs. Phase-locked averaged $T_e(R, \xi)$ contour (c) before and (d) after an ELM. (e) $T_e(R)$ across the island O-point before and after an ELM. Figures (c), (d) and (e) are adapted from L. Bardóczi *et al.*, Phys. Plasmas **24**, 062503 (2017), with the permission of AIP Publishing.

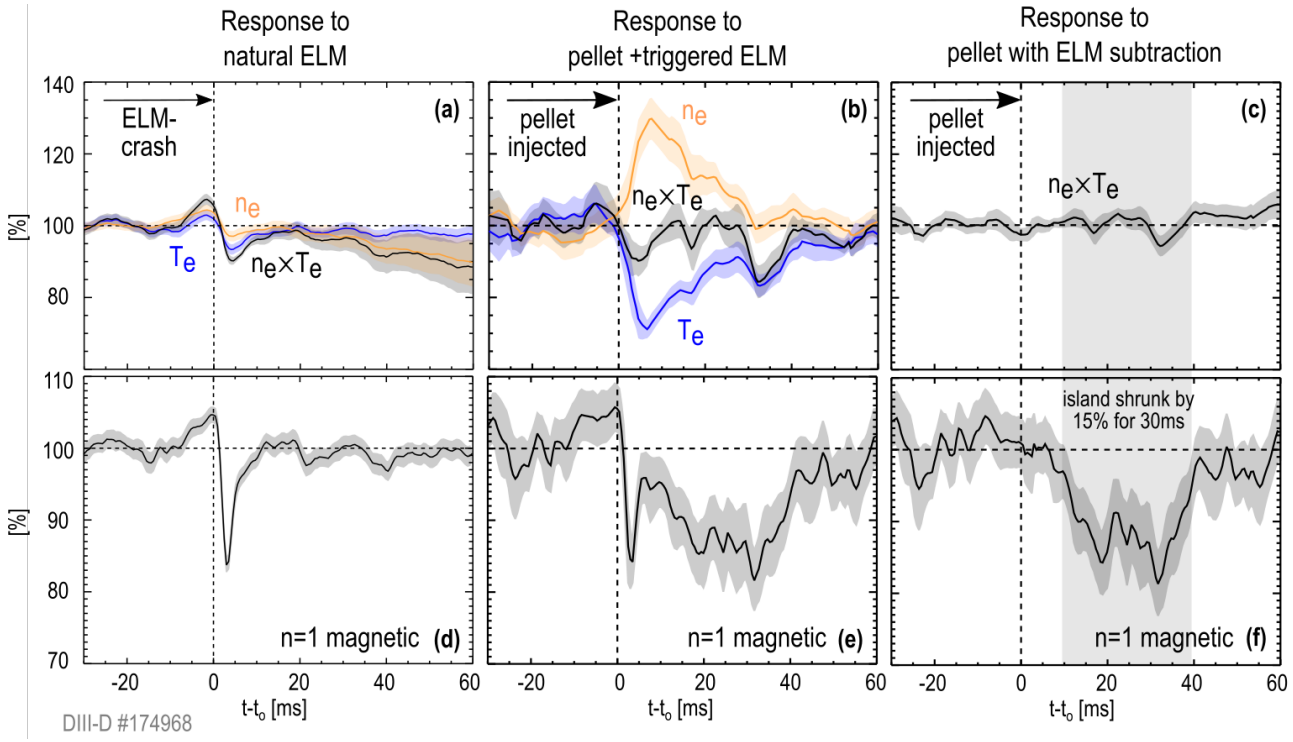

FIG. 3: phase-lock averaged n_e, T_e at $q = 2$ and $n_e \times T_e$ to (a) ELM times, (b) pellet injection times. (c) Difference between $n_e \times T_e$ during pellets and ELMs. phase-lock averaged $n = 1$ Mirnov amplitude to (d) ELM times, (e) pellet injection times. (f) Difference between $n = 1$ Mirnov amplitude during pellets and ELMs.

toroidal angles, respectively. Figs. 2 (c) and (d) show the $T_e(R, \xi)$ contours across the island *before* and *after* the ELM, respectively. Increase of ∇T_e inside the island *after* the ELM is indicated by the fact that the T_e contours are more dense compared to *before* the ELM. Interestingly, when 1.7W/cm^3 EC power is deposited in the island region in the same discharge, the power balance $\chi_\perp$ of the background plasma (calculated with TRANSP) increases from 1.7 m^2/s to 5m^2/s. At the same time, the drop of T_e at $q = 2$ as well as the drop of the $n = 1$ magnetic signal approximately doubles (not shown), hence the EC heating and/or current drive enhances the NTM response to ELMs. Increased ∇T_e inside the island 5 ms after the ELM, compared to 2 ms before the ELM, is more clearly shown in the $T_e(R, \xi = \pi)$ radial profiles across the O-point in Fig. 2 (e). Ensemble averaging the data over 11 (24) ELMs in the window with (without) EC heating and current drive shows that ∇T_e increases by 52eV/cm $\pm$ 29% (12eV/cm $\pm$ 41%) at the island separatrix in line with the O-point (R = 207.9 cm, $\xi = \pi$) due to ELMs.

Similarly to the above described lower density shots,

the n_e and T_e perturbations caused by ELMs both propagate to $q = 2$ in the discharges with pellets and cause n_e (T_e) to drop by about 5% (10%) [Fig. 3 (a)]. In sync, the $n = 1$ magnetic signal drops with a similar character as in the low density shot [Fig. 3 (d)]. Here the n_e, T_e and $n = 1$ magnetic signal were phase-lock averaged within the flat top phase of a single discharge (DIII-D #174968), where 70 ELMs and 8 pellets were available for the analysis. The uncertainty of the drop of the ensemble averaged n=1 signal is characterized by the precision of the mean before ELMs and after ELMs for which the $\bar{\sigma}$ standard error is the metric ($\bar{\sigma} = \sigma/\sqrt{N-1}$ where σ is the standard deviation and N is the sample size). $\bar{\sigma}$ is shown by the shaded regions in Fig. 3. The results shown in Fig. 3 are in quantitative agreement with two repeat discharges (DIII-D #174964 and #174965).

B. Triggered ELMs

In these experiments, the pellets triggered ELMs as seen from the fact that a D_α spike [Fig. 1 (k)] occurs in sync with the surge of n_e [Fig. 1 (g)] after each pellet. Further, drops in the $n = 1$ magnetic signal caused by ELMs in Fig. 3 (d) are also present at the pellet injection times in Fig. 3 (e). The relative growth rates of the most unstable peeling-ballooning modes calculated with ELITE[42] linear stability analysis (not shown) indicate that the plasma was unstable to peeling-ballooning modes just before injections, representative for DIII-D discharges in this parameter range[43]. Here the kinetic equilibria were reconstructed for the 80-99 % ELM phase during the same time window. The linear stability analysis of the equilibria before natural ELMs and before triggered ELMs is consistent with the observation that the ELM frequency is not increased significantly by the pellets. In addition, the decay rate of the associated D_α spike and the magnetic character in the Mirnov-data (not shown) all support that these events triggered by the fueling pellets are ELMs. Triggered ELMs, similarly to natural ELMs, lead to δT and δn perturbations that propagate to the $q = 2$ rational surface. As the effect of pellet ablation and triggered ELM take place on different time-scales, their effect on the 2/1 NTM can therefore be readily separated, see Subsection III C.

C. Effect of pellets

The $n = 1$ magnetic signal phase-locked to natural ELM times in Fig. 3 (d) shows that the NTM amplitude shrinks typically by about 17% due to ELMs in the pellet experiment. Simultaneously, both n_e and T_e drop at $q = 2$, which results in a drop of β_e [Fig. 3 (a)]. Here $\beta_e \propto n_e T_e$ is the β of electrons at $q = 2$.

After pellet injection, n_e increases and T_e drops by about 30%. The $n_e T_e$ product in Fig. 3 (b) is nearly constant with small drops comparable to those caused by natural ELMs in Fig. 3 (a). In sync, the $n = 1$ magnetic signal drops initially by 15% and recovers in 10 ms [Fig. 3 (e)]. This initial drop is caused by the triggered ELM and is very similar to that caused by the natural ELM [Fig. 3 (d)]. Later on, a second drop develops in the $n = 1$ magnetic signal starting around 10 ms after the pellet which lasts for about another 30 ms.

To isolate the effect of the pellet from the triggered ELM, the $n = 1$ magnetic response to ELMs ($n = 1$ phase-locked to natural ELMs [Fig. 3 (d)]) is subtracted from the $n = 1$ response to pellets ($n = 1$ phase-locked to pellets [Fig. 3 (e)]), see [Fig. 3 (f)]. Recall that both of the phase-locked signals were calculated in the flat top phase of the same discharge. This shows that the second, long-term shrinking of the island is the only effect of the pellet-caused perturbation. Similarly, the difference between β_e phase-locked to ELMs from β_e phase-locked to pellets shows that the pellet alone does not lead to significant changes in the local β_e at $q = 2$ [Fig. 3 (c)]. Analysis of the $n = 1$ frequency shows that the island rotation follows a similar trajectory as the amplitude with an average drop of about 10% (not shown). Possible explanations of these observations are discussed in Section IV.

D. NTM partial stabilization due to pellets in KSTAR

The DIII-D observation of NTM partial stabilization by fueling pellets was also tested in KSTAR H-mode plasmas. The relevant plasma parameters were: $R_o = 1.8$ m, $a = 0.5$ m, $B_T = 1.8$ T, $I_p = 400$ kA, $q_{95} \approx 6.2$. These

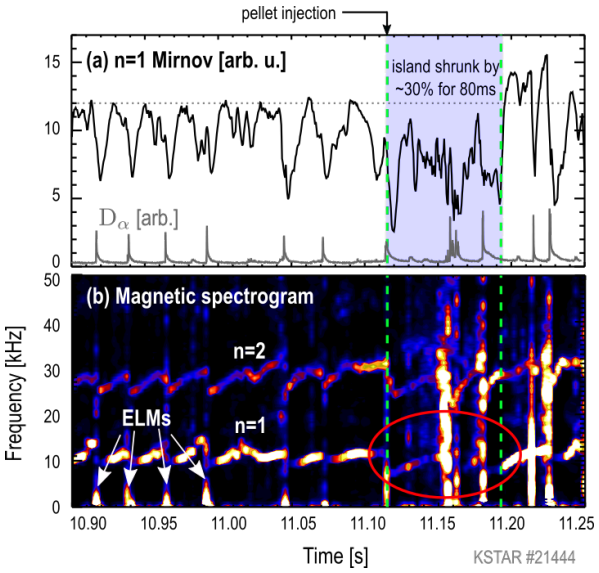

FIG. 4: (a) Time history and (b) spectrogram of the $n = 1$ Mirnov amplitude during pellet injection in KSTAR.

plasmas developed an $n = 1$ magnetic mode rotating with 10 kHz frequency, which is consistent with a 2/1 NTM. The major radius coordinate of $q = 2$ is expected to be in the $R_{q=2} = 1.9 - 2.0$m range based on EFIT constrained

by the motional Stark effect diagnostic (MSE[44]). Based on Mirnov data, the width of these islands is expected to be $W = 2-3$ cm, which is significantly smaller than the DIII-D 2/1 islands. Deuterium pellets with cylindrical shape (2 mm diameter and 1.5 mm length) were injected from the high field side at near 20 degree poloidal angle and entered the plasma with an average speed of 211 m/s. Reduction of the 2/1 island amplitude after pellet injection is seen from the time history of the $n = 1$ Mirnov amplitude with the most significant response after the injection at about 11.15 s in Fig. 4. Here the $n = 1$ signal briefly shrinks and recovers after ELMs as in the DIII-D discharge and then shrinks by about 30% for about 80 ms at the time of the pellet injection. Broadband magnetic fluctuations increase during this time window. This data demonstrates that the pellet has a stabilizing effect on the 2/1 mode in the KSTAR plasma, in line with the DIII-D results.

Due to limited diagnostics accessibility, further analysis in the KSTAR plasmas is not attempted. Investigation of physics origins of the partial stabilization is based upon DIII-D data in Section IV and thereafter.

IV. POTENTIAL PHYSICS ORIGINS OF PARTIAL STABILIZATION OF THE 2/1 NTM DUE TO PELLETS

As mentioned in Section I, partial stabilization of the 2/1 NTM due to pellets can not be explained by (i) a change in the classical stability parameter Δ', (ii) a rotation drop or (iii) a resistivity surge ($\eta \propto T_e^{-3/2}$), but is consistent with (iv) increased cross-field transport ($\chi_\perp$) at the island O-point.

Some of these effects can be discussed within the framework of the Modified Rutherford equation that prescribes NTM evolution. The simplest form including classical stability (first term), the neoclassical bootstrap current drive (second term) and the ECCD current (third term) reads:

$$\frac{dW}{dt} = \frac{\eta}{\mu_\circ}\Delta' + \frac{\eta}{\mu_\circ}\frac{D_{NC}W}{W^2 + L_\chi^2} + p_\alpha \frac{\alpha_\circ}{W} \qquad (1)$$

Here $\mu_\circ$ is the vacuum permittivity, $D_{NC} \propto j_{BS} \propto \nabla p$ is the neoclassical bootstrap current drive and L_χ is the cross-field electron thermal transport length-scale (recall that $L_\chi \propto \chi_\perp^{1/4}$). $\alpha_\circ$ is a constant negative parameter quantifying the magnitude of externally driven j_{ECCD} at the O-point at complete stabilization. p_α is then a dimensionless parameter between 0 (no j_{ECCD}) and 1 (complete stabilization).

(i) Classical stability. The islands shrink about 10 ms after injections, which is much faster then the timescale required for the current profile to evolve. Therefore, it can be assumed that Δ' is nearly constant when the island shrinks due to the pellets.

(ii) Rotation. Former DIII-D experiments[45] reported a decreased β threshold for 2/1 NTM onset at lower rotation, implying that 2/1 NTMs are more unstable at lower rotation. The pellets are injected radially, increasing the plasma density, without delivering angular momentum. This reduces the plasma rotation which then decreases the island frequency. Therefore, based on earlier studies, the reduction of island frequency due to the pellets can not explain the observed partial stabilization.

(iii) Temperature. Drops in T_e increase η, which in turn increases the growth rate classically and neoclassically. Considering these two terms, the saturated island width (W_{SAT}) is independent of η (at $j_{ECCD} = 0$). Therefore, a change in η due to the drop in T_e can not explain the shrinking of the island. In addition to the above, a drop in T_e in the island O-point region could also drive the NTM more unstable through radiation[46].

(iv) Turbulent transport. Increased $\tilde{n}$ enters the MRE through L_χ, the boundary layer inside the island where gradients are maintained[15], which can vary in the 1.2 - 4 cm range, as reported previously[40]. This reduces the size of the T_e flat spot at the O-point region compared to the size of the magnetic island, reducing the destabilizing δj_{BS}. W_{SAT} is given by the stable root of $dW/dt = 0$. The relative change of W_{SAT} (at $j_{ECCD} = 0$) due to a change in L_χ is approximately:

$$R_W = \frac{\bar{L}_\chi^2/W_\circ^2}{1 + \bar{L}_\chi^2/W_\circ^2}\left(1 - \sqrt{R_\chi}\right). \qquad (2)$$

Here $W_\circ$ is the unperturbed island width, $L_\chi = \bar{L}_\chi(\chi_{turb.}/\chi_{neocl.})^{1/4}$ and $R_\chi = \chi_{turb.}/\chi_{neocl.} \approx 10^2$. $\bar{L}_\chi$ is the boundary layer in the unperturbed island and the ratio of transport coefficients was measured in earlier work[14]. Under these conditions, equation 2 estimates that W_{SAT} can shrink by up to about 20% due to a $\chi_\perp$ enhancement inside the island, which is in quantitative agreement with the observations of Section III. We note that the modified transport may also influence the j_{ECCD} directly[47,48], which is neglected here for simplicity.

In the following, profile and turbulence data analyses as well as gyrokinetic simulations with magnetic islands will be in the focus of the paper. DIII-D data and GENE simulations qualitatively support the hypothesis that pellet–induced turbulent transport enhancement near the O-point causes islands to shrink.

V. EVOLUTION OF PLASMA PROFILES AND TURBULENCE DURING THE PELLET CYCLE

In this section, we first present measurements of density profiles and temperature gradients [Subsection V A]. The pellets lead to increased gradients in the island region, which are turbulence drives, hence $\tilde{n}$ increase in the island region is expected. This is followed by GENE linear stability analysis, showing significant increase of Micro Tearing Mode and Trapped Electron Mode growth rates in the island region due to the pellet [Subsection V B]. These are consistent with Beam Emission Spectroscopy measurements of $\tilde{n}$ inside the island

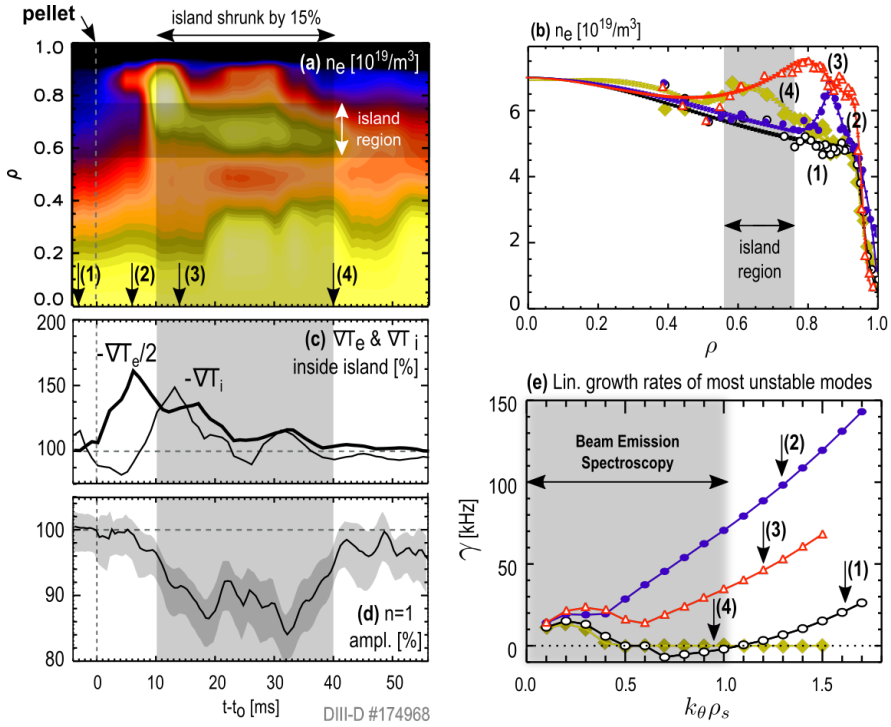

FIG. 5: (a) Spatiotemporal evolution of the rotation averaged electron density (n_e, Thomson scattering). (b) Radial profiles of the rotation averaged n_e during the pellet cycle at 4 different times: (1) 3 ms before pellet injection, (2) 6 ms after injection, after start of ablation, (3) 14 ms after injection at maximum n_e perturbation and (4) 40 ms after injection when the perturbations have mostly decayed. The solid lines represent cubic spline fits to the data points. Evolution of rotation averaged (c) $-\nabla T_e$ and $-\nabla T_i$ at $q = 2$. (d) Phase-locked $n = 1$ signal (repeat of Fig. 3 (f) for reference). (e) Linear growth rates of most unstable micro-instabilities (micro tearing modes) at $q = 2$ via GENE during the pellet cycle.

showing increased low-k turbulence after the pellet [Subsection V C].

A. Plasma profiles

The $n_e(t, \rho)$ contour in Fig. 5 (a) shows that in response to the pellet δn_e propagates radially inward until it reaches the island region ($\rho \approx 0.59 - 0.79$) where it is confined for about 30 ms. This transport behavior is qualitatively similar to that reported in 1/1 RMP islands in LHD[27]. $n_e(\rho)$ profiles at 4 different times are shown in Fig. 5 (b). These 4 times are:

- t_1 : 3 ms before injection (reference). The plasma is in equilibrium and ∇n_e is small inside the island region.
- t_2 : 6 ms after injection; max. of $-\nabla T_e$ at $q = 2$. When the pellet starts ablating, a peak develops first at the top of the pedestal around $\rho = 0.87$ which then grows and propagates inward.
- t_3 : 14 ms after injection; max. of $-\nabla T_i$ at $q = 2$. The contour of $n_e(t, \rho)$ [Fig. 5 (a)] and the $n_e(\rho)$ profiles [Fig. 5 (b)] show that ∇n_e is reversed inside the island region at this time. This implies a reduced δj_{BS} drive of the NTM.
- t_4 : 40 ms after injection; max. of $-\nabla n_e$. $-\nabla T_e$ and $-\nabla T_i$ at $q = 2$ are about equal to before pellet injection.

Time traces in Fig. 5 (c) show that $-\nabla T_e$ increases first (t_2), followed by an increase in $-\nabla T_i$ inside the island region. Note that due to the short electron-electron collision time the drop in T_e is almost instantaneous, which is detected by the Thomson scattering diagnostic. In contrast, the thermalization of the pellet deuterium ions with the probed carbon impurity takes place on the much longer ion-ion collision time, which explains the delayed carbon impurity T_i response, as detected by the CER diagnostic. When the inward propagating density peak passes $q = 2$, ∇n_e increases temporarily until the n_e peak decays.

Note that ∇T_e and ∇T_i at $q = 2$ relax in about 40 ms as the perturbations propagate further in but it takes a longer time until the local T_e and T_i recover. The $n = 1$ amplitude recovers on the time-scale of the gradients.

MSE data is available during these shots, but measurement limitations seem to preclude direct measurement of current profile changes with the pellets. Due to the limited time response of the utilized lock-in amplifiers, the fast change in density and light intensity caused by a pellet leads to a transient spurious polarization measurement, i.e. the inferred pitch angle changes too much, too quickly to be physically real. This masks the actual local magnetic field response at the NTM rational surface.

As gradients are turbulence drives, it is expected that turbulence driven fluctuations increase after the pellet. The type and growth rates of the fastest growing micro-instabilities was calculated with linear GENE gyrokinetic simulations in Subsection V B.

B. Linearly unstable drift waves at $q = 2$ (GENE)

Determining the type of unstable drift-waves across the island requires nonlinear gyrokinetic simulations with magnetic islands and plasma parameters (T_e/T_i, ∇T_e,

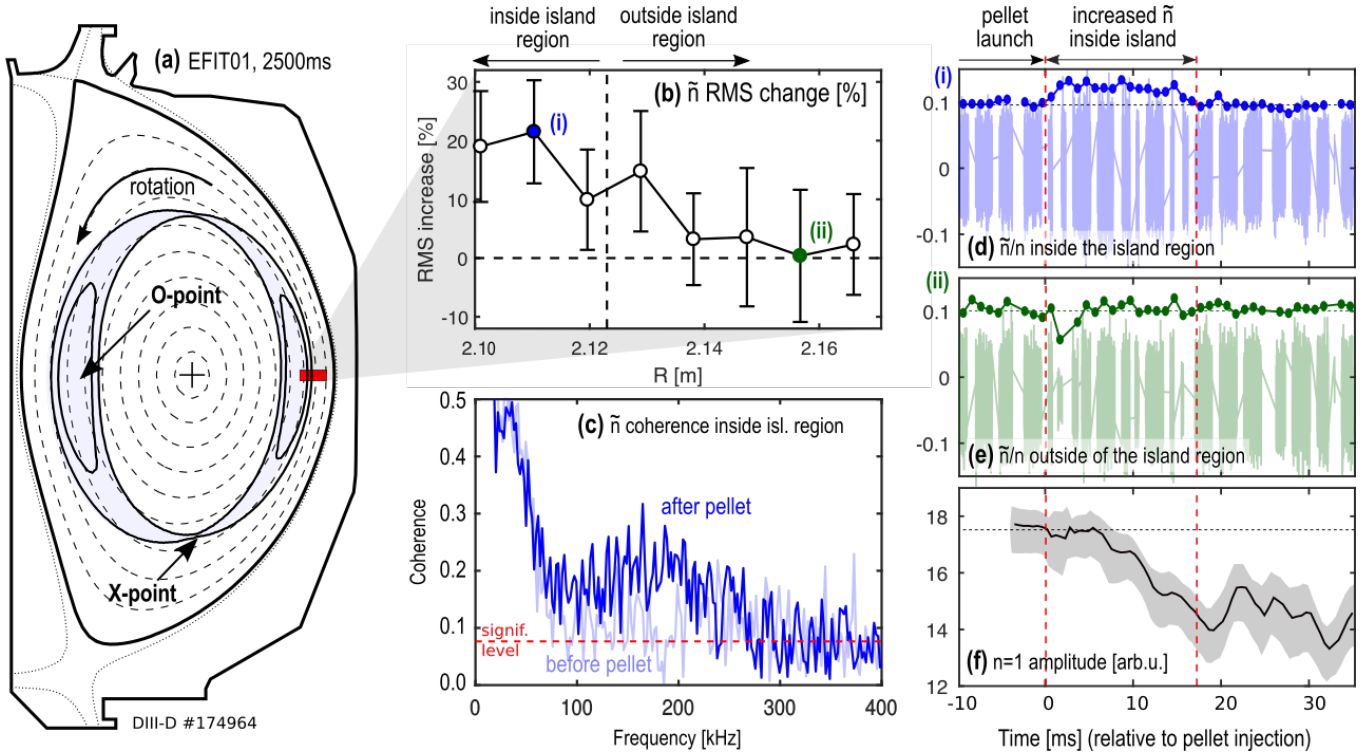

FIG. 6: Evolution of $\tilde{n}$ inside and nearby the $m/n = 2/1$ islands after pellet injections as detected by the BES diagnostic. (a) Magnetic equilibrium with an illustration of the 2/1 islands, indicating their location and width, and BES probing locations. (b) Radial profile of the change of $\tilde{n}$ RMS due to the pellet. (c) $\tilde{n}$ coherence inside the island region calculated from poloidally adjacent BES channels inside the island region (R $\approx$ 2.11m). Time histories of $\tilde{n}/n$ (d) inside and (e) outside the island region, respectively. (f) n=1 magnetic amplitude (repeat of Fig. 3 (f) for reference).

∇T_i, ∇n, geometry, rotation, etc.) carefully matched to the experiment, which is beyond the scope of this paper. However, in order to identify the type of dominant micro-instability of the background plasma at $q = 2$ during pellet injections, we conducted linear GENE gyrokinetic simulations[32] [FIG. 5 (e)] using 4 sets of experimental profiles at the time-slices $t_1 - t_4$ discussed in Subsection V A. Input are the experimentally measured n_e T_e, T_i, carbon impurity rotation profiles and the reconstructed magnetic equilibrium. These profiles are time averaged over multiple island rotation cycles including the X-point and the O-point. As such, the simulation can only give a general idea of the type of most unstable modes of the background plasma and their linear growth rates during the pellet cycle. These flux-tube simulations were run on the ion-scale ($k_\theta \rho_s = 0.1 - 17.0$), used two fully kinetic species (deuterons and electrons) and included electromagnetic effects. Here k_θ is the poloidal wavenumber and $\rho_s = c_s/\omega_i \approx 0.4$ cm, where $c_s = \sqrt{T_e/m_i}$, and m_i and ω_i are the ion mass and cyclotron frequency, respectively. The dominant instability at $k_\theta \rho_s < 0.6$ is the Micro Tearing Mode (MTM) [Fig. 5 (e)], which are stable when electromagnetic effects are removed (i.e. when Ampére's law is not evolved) and they are sensitive to both ∇T_e and ∇T_i. The dominant instability at $k_\theta \rho_s > 0.6$ is the Trapped Electron Mode (TEM), which are sensitive to collisionality and propagate in the electron diamagnetic direction.

The Beam Emission Spectroscopy[49] diagnostic is sensitive in the $k_\theta \rho_s < 1.0$ range. Hence, $\tilde{n}$ probed by this diagnostic is in the expected range of MTM and TEM turbulence.

C. Evolution of low-k turbulence (BES)

The BES system[49] provides radially resolved measurements of $\tilde{n}$ locally by measuring the light emission from the neutral beam at $\phi = 150°$, 3.6 cm above the midplane across the 2/1 island region [Fig. 6 (a)]. This system is sensitive to localized, long-wavelength $\tilde{n}$ of $k_\theta < 1$ cm^{-1} which is the expected wavenumber range of the MTM instability in these plasmas. The typical separation between the channels is about 1 cm, the radial and poloidal localization is about 1 cm.

The BES system detects increased turbulence intensity ($\tilde{n}^2$) by 20% inside the island region, after the pellet (compared to $\tilde{n}^2$ before the pellet). This is seen in the radial profile of the $\tilde{n}$ RMS increase in Fig. 6 (b). Coherence spectra of 50 ms windows between vertically adjacent channels inside the island show that the increase of $\tilde{n}$ is in the broad and high frequency $\Delta f = 100 - 200$ kHz range, which is consistent with increased broadband turbulence inside the island resulting from pellet injection

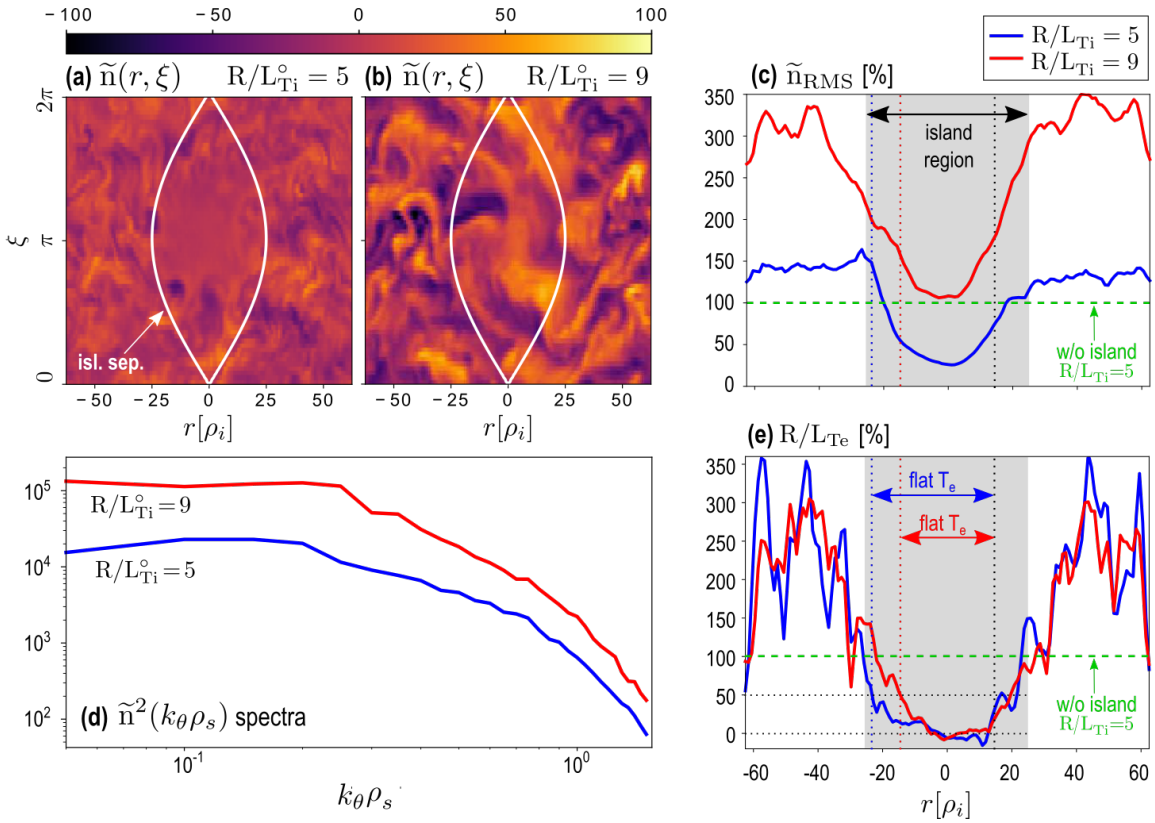

FIG. 7: Non-linear GENE gyrokinetic ITG turbulence simulations with static magnetic islands. Snapshot of instantaneous density fluctuations at (a) $R/L_{T_i}=5$, (b) $R/L_{T_i}=9$. (c) Radial profiles of $\widetilde{n}$ through the O-point.(d) k_θ-spectra of $\widetilde{n}$ outside of the island at r=-54 ρ_i. (e) Radial profiles of R/L_{T_e} through the O-point.

[Fig. 6 (c)]. Here only ELM-free windows are analyzed, when the modulated neutral beam was on. Example time trances of $\widetilde{n}^2$ inside and outside the island are shown in Fig. 6 (d) and (e), respectively. The $n=1$ magnetic amplitude [Fig. 6 (f)] starts to decrease when $\widetilde{n}^2$ is increased inside the island. This suggests a multi-scale interaction between low-k $\widetilde{n}$ and the 2/1 NTM. However, this data does not fully explain the observations as the the island remains shrunk for about 30 ms (as long as local gradients are modified) even after the BES $\widetilde{n}^2$ has decayed back to the level of before pellet injection. Possible explanations include (i) increase of intermediate-k turbulence during the whole 30 ms window which is not detected by BES, (ii) the resistive time-scale of the NTM evolution restraining instantaneous island recovery.

VI. LOW-k TURBULENCE SPREADING INTO MAGNETIC ISLANDS IN GYROKINETIC SIMULATIONS

To investigate causality between elevated gradients outside of the island, turbulence spreading into the island and reduced NTM drive, we used static magnetic islands in GENE nonlinear gyrokinetic turbulence simulations in 3-dimensional, toroidal geometry. This is accomplished by qualitatively testing if increased background gradients can lead to stronger turbulence spreading into the magnetic island O-point region and if this effect shrinks the area where the temperature is flat. The islands are implemented through the parallel component of the vector potential[50]. GENE self-consistently solves the gyrokinetic-Maxwell system of equations on a fixed

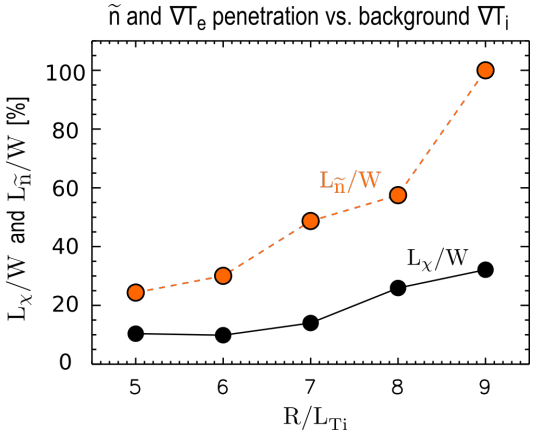

FIG. 8: Scaling of boundary layer width L_χ (where $\nabla T_e > \nabla T_e^{ref}/2$) and turbulence penetration depth $L_{\widetilde{n}}$ (where $\widetilde{n} \approx \widetilde{n}^{ref}$) vs background ion temperature gradient R/L_{T_i} in GENE non-linear gyrokinetic simulation with a magnetic island.

grid in five dimensional phase space (plus time). Two particle species (deuterons and electrons) were used including electromagnetic effects. The equilibrium magnetic configuration (large aspect-ratio, circular model equilibrium) is characterized by a safety factor of $q = 1.5$, magnetic shear of $\hat{s} = 0.16$ and inverse aspect ratio of $\epsilon = 0.19$. In our reference simulation $R/L_n = 2.2$ and $R/L_{T_e} = R/L_{T_i} = 5$ ($R/L_{T_i} = R/(T_i/\partial_r T_i)$ and similar definitions hold for R/L_n and R/L_{T_e}). These equilibrium parameters are similar to the "Cyclone DIII-D base case parameter set"[51] (discharge #81499) as in other gyrokinetic simulations[52,53], where the most unstable micro-instability is the Ion Temperature Gradient (ITG) mode. For clarity, we point out that the studied NTM in the DIII-D pellet experiment is characterized by $m/n = 2/1$ mode numbers and the dominant linearly unstable drift waves at $q = 2$ of the background plasma are the MTM and the TEM instabilities , see Section II and Section V B, respectively. Conducting nonlinear gyrokinetic simulations with magnetic islands and input parameters (T_e/T_i, ∇T_e, ∇T_i, ∇n, geometry, rotation, etc.) carefully matched to a specific experiment would require extensive simulation effort which is beyond the scope of this paper. These simulations therefore only qualitatively test if increased background gradients can lead to stronger turbulence spreading into the magnetic island O-point region and if this effect shrinks the temperature flat spot.

The first comparison of GENE turbulence simulations with magnetic islands to DIII-D turbulence data showed that GENE can qualitatively reproduce the measured scaling of $\tilde{n}$ modifications inside and outside the island with respect to the island width[17]. Here we attempt to model the effect of the pellet only on the dominant instability drive near the island, ∇T_i, hence a set of simulations in the experimentally relevant range of $R/L_{T_i} = 5 - 9$ are comducted, where $R/L_{T_i} = 5$ and 9 correspond to "*before pellet*" and "*after pellet*", respectively. The simulations are started with uniform gradients where ITG modes are unstable. Next, turbulence, transport and the profile perturbations are evolved self-consistently on a much longer time-scale than the turbulence correlation time, after the system has reached statistical equilibrium.

Snapshots of the instantaneous $\tilde{n}(r, \xi)$ in the saturated state show that $\tilde{n}$ is reduced in the vicinity of the O-point when $R/L_{T_i} = 5$ [Fig. 7 (a)] but $\tilde{n}$ spreads into the O-point region when $R/L_{T_i} = 9$ [Fig. 7 (b)]. Radial profiles of $\tilde{n}_{RMS}$ (the RMS of $\tilde{n}$) across the O-point [Fig. 7 (c)] show that $\tilde{n}$ is increased by 40% outside and decreased by 75% inside the island when $R/L_{T_i} = 5$. In contrast, when $R/L_{T_i} = 9$, $\tilde{n}$ is increased by a factor of 3 outside the island, and $\tilde{n}$ is nearly unchanged at the O-point due to increased $\tilde{n}$ penetration into the island [Fig. 7 (c)]. Here we define $L_{\tilde{n}}$ as the width of the boundary layer inside the island separatrix, where $\tilde{n}$ is equal to $\tilde{n}$ of the reference simulation without pellet and without island. Time averaged helical k-spectra $\langle \tilde{n}(k_\xi) \rangle_t$ in Fig. 7 (d) show that ITG modes are more unstable primarily in the lower-k part of the spectrum. This increases the radial correlation length of $\tilde{n}$, which then offers an explanation of increased $\tilde{n}$ penetration into the island.

As expected, increased $\tilde{n}$ is accompanied by increased ∇T_e in the boundary layer inside the island separatrix [Fig. 7 (e)]. Here we define L_χ as the width of the boundary layer inside the island separatrix, where ∇T_e is maintained at least at a 50% level of the reference simulation.

The scaling of L_χ and $L_{\tilde{n}}$ vs R/L_{T_i} in Fig. 8 shows that $\tilde{n}$ and ∇T_e gradually increase inside the island separatrix as the background ∇T_i is increased. As R/L_{T_i} is increased from 5 to 9, $\tilde{n}$ at the O-point increases to that of the background plasma (w/o island and w/o pellet) and L_χ widens by a factor of 3, reducing the T_e flat spot at the O-point to about 70% of W. Therefore, these gyrokinetic turbulence simulations with magnetic islands demonstrate the causality between reduced NTM drive and elevated background gradients through turbulence spreading. This simulation result makes it conceivable that the increased $\tilde{n}$ inside the island detected by BES can be responsible for the shrinking of the NTM in the presented DIII-D experiment.

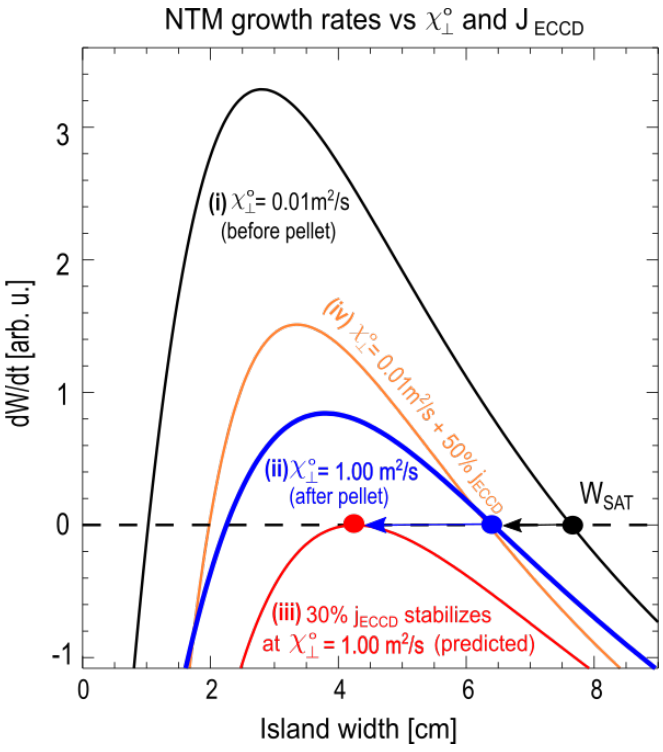

FIG. 9: Solutions of the modified Rutherford equation (eq. 1): (i) w/o pellet w/o j_{ECCD}, (ii) w pellet w/o j_{ECCD} and (iii) w pellet w 30% j_{ECCD} (relative to required j_{ECCD} for complete stabilization w/o pellet). (iv) Shows the solution w/o pellet w 50% j_{ECCD} for comparison with (ii). Saturation points are marked with circles and parameters of (i) are fit to match the measured W_{SAT} in equilibrium.

VII. IMPACT OF PERPENDICULAR TRANSPORT ON j_{ECCD} REQUIREMENTS FOR NTM STABILIZATION

NTM growth rates calculated from equation 1 are depicted in Fig. 9. The growth rate in equilibrium before pellet injection is shown by (i), where W_{SAT} = 8 cm (matched to experiment), $p_\alpha = 0$ (no j_{ECCD}) and the cross-field thermal transport coefficient at the O-point is $\chi_\perp^\circ = 10^{-2}\mathrm{m}^2/\mathrm{s}$. Increasing $\chi_\perp^\circ$ to the level of the background plasma transport ($\chi_\perp^\circ = 1\mathrm{m}^2/\mathrm{s}$) leads to the shrinking of W_{SAT} by 20% (ii), in quantitative agreement with the experiment reported in Section III.

In comparison, (iv) 50% j_{ECCD} has the equivalent effect on W_{SAT} as the pellet. This 50% is relative to the amount of j_{ECCD} needed for complete stabilization w/o pellet (i.e. $p_\alpha = 0.3$). Interestingly, with transport enhancement (iii) ($\chi_\perp^\circ = 1\mathrm{m}^2/\mathrm{s}$), only 30% of j_{ECCD} is enough for complete stabilization of the 2/1 island. In this case the island self-stabilizes at W $\approx$ 4.5 cm. This indicates that a fueling pellet can significantly reduce the gyrotron requirements for the stabilization of NTMs.

Increasing j_{ECCD} leads to smaller W until the marginally stable point is reached and the island self-stabilizes (marked with circles), as shown in Fig. 10 (a) at three different values of $\chi_\perp^\circ$. Note that increasing the transport by a factor of 100 has three consequences: (i) W shrinks by up to 20% when j_{ECCD}=0, (ii) W decreases more rapidly as j_{ECCD} is increased and (iii) the self-stabilizing W increases from 4 cm to about 4.5 cm. These 3 beneficial effects combine to reduces the j_{ECCD} requirement for NTM stabilization to 30%.

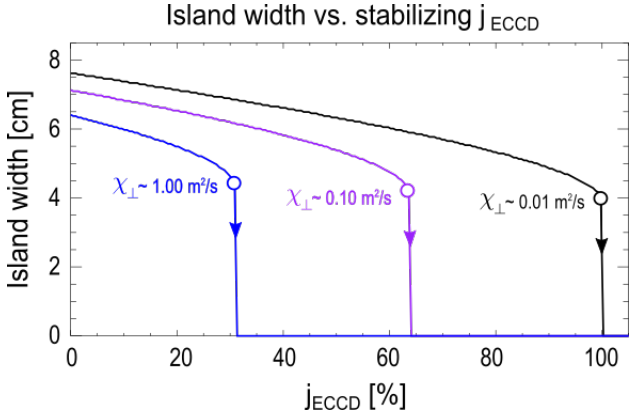

FIG. 10: Island width after applying j_{ECCD} with $\chi_\perp = 1\ \mathrm{m}^2/\mathrm{s}$, $\chi_\perp = 0.1\ \mathrm{m}^2/\mathrm{s}$ and $\chi_\perp = 0.01\ \mathrm{m}^2/\mathrm{s}$ at the O-point.

VIII. SUMMARY

Controlled partial stabilization of core $m/n = 2/1$ Neoclassical Tearing Modes (NTMs) by fueling deuterium pellets is demonstrated in H-mode plasmas in the DIII-D and KSTAR tokamaks. In the framework of non-linear NTM theory, this observation can not be explained by classical stability, resistivity surge or rotation drop caused by the pellet, but is consistent with increased cross-field transport at the island O-point. When the pellet–induced thermal perturbation (δT) reaches the island in DIII-D, local low-k turbulence ($\tilde{n}$) increases and the island shrinks. This $\tilde{n}$ is in the expected range of the MTM and TEM instabilities (GENE). When the pellet–induced perturbations decay, $\tilde{n}$ restores to the normal level and the island recovers. Complementing the experimental data, non-linear GENE gyrokinetic simulations with magnetic islands qualitatively support that increased background temperature gradients can increase $\tilde{n}$ spreading into the O-point region. This can enhance the cross-field transport across the island separatrices and thereby reduce the NTM drive. The change in saturated island width resulting from transport enhancement at the O-point in the MRE shows quantitative agreement with the experiment. Furthermore, the MRE predicts significant reduction of the j_{ECCD} requirement for complete NTM stabilization when the transport is enhanced at the island O-point.

As NTMs are non-linear instabilities with a threshold island width of a few centimeters, NTMs self-stabilize when the island width shrinks below the threshold. After stabilization, the discharge may run NTM free until a large enough trigger destabilizes the NTM again. In such event, the suppression procedure must be repeated as in the"catch and subdue" (C&S) control method[9]. In C&S the gyrotrons track the $q = m/n$ surface using real-time mirror steering and the island is suppressed by turning the ECCD on when the NTM amplitude exceeds a threshold. C&S is more cost efficient than "preemptive" stabilization (where the ECCD is constant on and aiming at $q = m/n$). C&S NTM control with combined ECCD & pellet may offer a path toward further reducing the j_{ECCD} needed for complete NTM stabilization.

Active NTM control with low gyrotron power is desirable, as it can (i) improve the net electricity output of future reactors, (ii) can free up gyrotrons for heat and current drive elsewhere in the plasma and (iii) can extend the active NTM control solution via ECCD to operational regimes where the current drive efficiency is low. In particular, in ITER startup operations, EC current drive efficiency at $q = 2$ at the second harmonic resonance is predicted to be lower due to partial absorption of the EC waves at the third harmonic resonance in the edge. Further experiments with j_{ECCD} scans have been proposed in DIII-D to explore the potential of combined pellet - j_{ECCD} control of the 2/1 NTM.

ACKNOWLEDGEMENTS

The authors would like to thank Francesca Turco and Christopher T. Holcomb for very useful discussions.

This research was supported by the General Atomics Postgraduate Research Participation Program administered by ORAU. This material is based upon work sup-

ported by the U.S. Department of Energy, Office of Science, Office of Fusion Energy Sciences, using the DIII-D National Fusion Facility, a DOE Office of Science user facility, under Award [1]DE-FC02-04ER54698. DIII-D data shown in this paper can be obtained in digital format by following the links at https://fusion.gat.com/global/D3D_DMP. This report was prepared as an account of work sponsored by an agency of the United States Government. Neither the United States Government nor any agency thereof, nor any of their employees, makes any warranty, express or implied, or assumes any legal liability or responsibility for the accuracy, completeness, or usefulness of any information, apparatus, product, or process disclosed, or represents that its use would not infringe privately owned rights. Reference herein to any specific commercial product, process, or service by trade name, trademark, manufacturer, or otherwise does not necessarily constitute or imply its endorsement, recommendation, or favoring by the United States Government or any agency thereof. The views and opinions of authors expressed herein do not necessarily state or reflect those of the United States Government or any agency thereof.

The GENE gyrokinetic computations have been carried out at the MARCONI-Fusion supercomputer at CINECA, Italy.

KSTAR experiments were supported by Korea Ministry of Science and ICT under NFRI R&D programs (NFRI-EN1901-10 and NFRI-EN1941-5).

REFERENCES

[1]O. Sauter, R. J. La Haye, Z. Chang, D. A. Gates, Y. Kamada, H. Zohm, A. Bondeson, D. Boucher, J. D. Callen, M. S. Chu, T. A. Gianakon, O. Gruber, R. W. Harvey, C. C. Hegna, L. L. Lao, D. A. Monticello, F. Perkins, A. Pletzer, A. H. Reiman, M. Rosenbluth, E. J. Strait, T. S. Taylor, A. D. Turnbull, F. Waelbroeck, J. C. Wesley, H. R. Wilson, and R. Yoshinof. Beta limits in long-pulse tokamak discharges. *Phys. Plasmas*, 4:1654, 1997.

[2]R.J. La Haye, P.A. Politzer, and D.P. Brennan. Beta limit due to m/n=2/1 tearing mode onset in the diii-d hybrid scenario. *Nuclear Fusion*, 48:015005, 2008.

[3]R. Carrera, R. D. Hazeltine, and M. Kotschenreuther. Island bootstrap current modification of the nonlinear dynamics of the tearing mode. *Phys. Fluids*, 29(899), 1986.

[4]C.C. Petty, R.J. Jayakumar, M.A. Makowski, C.T. Holcomb, D.A. Humphreys, R.J. La Haye, T.C. Luce, P.A. Politzer, R. Prater, M.R.Wade, and A.S.Welander. Spatiotemporal changes in the pressure-driven current densities on diii-d due magnetic islands. *Nucl. Fusion*, 52(013011), 2012.

[5]C. C. Petty, M. E. Austin, C. T. Holcomb, R. J. Jayakumar, R. J. La Haye, T. C. Luce, M. A. Makowski, P. A. Politzer, and M. R. Wade. Magnetic-flux pumping in high-performance, stationary plasmas with tearing modes. *Phys. Rev. Lett.*, 102(045005), 2009.

[6]R. J. La Haye, S. Gunter, D. A. Humphreys, J. Lohr, T. C. Luce, M. E. Maraschek, C. C. Petty, R. Prater, J. T. Scoville, and E. J. Strait. Control of neoclassical tearing modes in diii-d. *Phys. Plasmas*, 9(5), 2002.

[7]C. C. Petty, R. J. La Haye, T. C. Luce, D. A. Humphreys, A. W. Hyatt, J. Lohr, R. Prater, E. J. Strait, and M. R. Wade. Complete suppression of the m=2/n=1 neoclassical tearing mode using electron cyclotron current drive in diii-d. *Nucl. Fusion*, 44(243), 2004.

[8]M. Maraschek, G. Gantenbein, T.P. Goodman, S. Günter, D.F. Howell, F. Leuterer, A. Mück, O. Sauter, H. Zohm, Contributors to the EFDA-JET Workprogrammea, and the ASDEX Upgrade Team. Active control of mhd instabilities by eccd in asdex upgrade. *Nucl. Fusion*, 45(11):1369–1376, 2005.

[9]A. S. Welander, E. Kolemen, R. J. La Haye, N. W. Eidietis, D. A. Humphreys, J. Lohr, S. Noraky, B. G. Penaflor, R. Prater, and F. Turco. Advanced control of neoclassical tearing modes in diii-d with real-time steering of the electron cyclotron current drive. *Plasma Phys. Control. Fusion*, 55(12), 2013.

[10]L. Figini. Electron cyclotron heating and current drive regimes in iter at reduced magnetic field strength. RFPPC, 2017.

[11]J. P. Meskat, H. Yohm, G. Gantenbein, S. Gunter, M. Maraschek, W. Suttrop, Q. Yu, and ASDEX Upgrade Team. Analysis of the structure of neoclassical tearing modes in asdex upgrade. *Plasma Phys. Control. Fusion*, 43(1325), 2001.

[12]J. A. Snape, K. J. Gibson, T. O'Gorman, N. C. Barratt, K. Imada, H. R. Wilson, G. J. Tallents, I. T. Chapman, and the MAST team. The influence of finite radial transport on the structure and evolution of m/n=2/1 neoclassical tearing modes on mast. *Plasma Phys. Control. Fusion*, 54(085001), 2012.

[13]M. J. Choi, G. S. Yun, W. Lee, H. K. Park, Y.-S. Park, S. A. Sabbagh, K. J. Gibson, C. Bowman, C. W. Domier, N. C. Luhmann Jr., J.-G. Bak, S. G. Lee, and the KSTAR Team. Improved accuracy in the estimation of the tearing mode stability parameters using 2d ecei data in kstar. *Nucl. Fusion*, 54(083010), 2014.

[14]L. Bardóczi, T. L. Rhodes, T. A. Carter, N. A. Crocker, W. A. Peebles, and B. A. Grierson. Non-perturbative measurement of cross-field thermal diffusivity reduction at the o-point of 2/1 neoclassical tearing mode islands in the diii-d tokamak. *Phys. Plasmas*, 23(052507), 2016.

[15]R. Fitzpatrick. Helical temperature perturbations associated with tearing modes in tokamak plasmas. *Phys. Plasmas*, 2:825, 1995.

[16]L. Bardóczi, T. L. Rhodes, T. A. Carter, A. Bañón Navarro, W. A. Peebles, F. Jenko, and G. McKee. Modulation of core turbulent density fluctuations by large-scale neoclassical tearing mode islands in the diii-d tokamak. *Phys. Rev. Lett.*, 116:215001, May 2016.

[17]L. Bardóczi, T. L. Rhodes, A. Bañón Navarro, C. Sung, T. A. Carter, R. J. La Haye, C. Petty, C. Crystal, and F. Jenko. Multi-field/-scale interactions of turbulence with neoclassical tearing mode magnetic islands in the diii-d tokamak. *Phys. Plasmas*, 24(056106), 2017.

[18]M.J. Choi, J. Kim, J.-M. Kwon, H.K. Park, Y. In, W. Lee, K.D. Lee, G.S. Yun, J. Lee, M. Kim, W.-H. Ko, J.H. Lee, Y.S. Park, Y.-S. Na, N.C. Luhmann Jr, and B.H. Park. Multiscale interaction between a large scale magnetic island and small scale turbulence. *Nuclear Fusion*, 57(12):126058, 2017.

[19]T. S. Hahm, P. H. Diamond, Z. Lin, K. Itoh, and S.-I. Itoh. Turbulence spreading into the linearly stable zone and transport scaling. *Plasma Phys. Control. Fusion*, 46(A323), 2004.

[20]X. Garbet. Radial propagation of turbulence in tokamaks. *Nucl. Fusion*, 34(963), 1994.

[21]K. Ida, T. Kobayashi, M. Ono, T. E. Evans, G. R. McKee, and M. E. Austin. Hysteresis relation between turbulence and temperature modulation during the heat pulse propagation into a magnetic island in diii-d. *Phys. Rev. Lett.*, 120(245001), 2018.

[22]A. Weller, A. D. Cheetham, A. W. Edwards, R. D. Gill, A. Gondhalekar, R. S. Granetz, J. Snipes, and J. A. Wesson. Persistent density perturbations at rational-q surfaces following pellet injection in the joint european torus. *Phys. Rev. Lett.*, 59(20), 1987.

[23]Y. Nagayama, G. Taylor, E. D. Fredrickson, R. V. Budny, A. C. Janos, D. K. Mansfield, K. M. McGuire, and M. Yamada. Tomography of (2, 1) and (3, 2) magnetic island structures on tokamak fusion test reactor. *Phys. Plasmas*, 3(2631), 1996.

[24]K. Narihara, K. Y. Watanabe, I. Yamada, T. Morisaki, K. Tanaka, S. Sakakibara, K. Ida, R. Sakamoto, N. Ohyabu, N. Ashikawa, M. Emoto, H. Funaba, M. Goto, H. Hayashi, H. Idei, K. Ikeda, S. Inagaki, N. Inoue, O. Kaneko, K. Kawahata, T. Kobuchi, A. Komori, S. Kubo, R. Kumazawa, S. Masuzaki, J. Miyazawa, S. Morita, O. Motojima, S. Murakami, S. Muto, T. Mutoh, Y. Nagayama, Y. Nakamura, H. Nakanishi, K. Nishimura, N. Noda, T. Notake, S. Ohdachi, Y. Oka, K. Ohkubo, M. Osakabe, S. Ozaki, B. J. Peterson, A. Sagara, K. Saito, H. Sasao, M. Sasao, K. Sato, M. Sato, T. Seki, T. Shimozuma, C. Shoji, S. Sudo, H. Suzuki, A. Takayama, M. Takechi, Y. Takeiri, N. Tamura, K. Toi, N. Tokuzawa, Y. Torii, K. Tsumori, T. Watari, H. Yamada, S. Yamaguchi, S. Yamamoto, K. Yamazaki, and Y. Yoshimura. Observation of the "self-healing" of an error field island in the large helical device. *Phys. Rev. Lett.*, 87:135002, Sep 2001.

[25]S. V. Annibaldi, P. Buratti, E. Giovanozzi, D. Frigione, and F. Porcelli. Enhanced central fuelling and m = 1 island formation after pellet ablation in the frascati tokamak upgrade. *Nucl. Fusion*, 44(1):12–19, 2004.

[26]E. Giovanozzi, S. V. Annibaldi, P. Buratti, D. Frigione, E. Lazarro, L. Panaccione, and O. Tudisco. Magnetic island structures and their rotation after pellet injection in ftu. *Nucl. Fusion*, 44(2):226–231, 2004.

[27]T.E. Evans, K. Ida, S. Ohdachi, K. Tanaka, M.W. Shafer, S. Inagaki, M.E. Austin, Y. Suzuki, E.A. Unterberg, the LHD, and DIII-D Experiment Groups. Comparative studies of static edge magnetic islands in diii-d and lhd. *IAEA*, 47(47073113), 2014.

[28]D. Terranova, F. Auriemma, A. Canton, L. Carraro, R. Lorenzini, and P. Innocente. Experimental particle transport studies by pellet injection in helical equilibria. *Nucl. Fusion*, 50(035006), 2010.

[29]J. L. Luxon. A design retrospective of the diii-d tokamak. *Nucl. Fusion*, 42(614), 2002.

[30]Y.-K. Oh, S. Yoon, Y.-M. Jeon, W.-Ha Ko, S.-Ho Hong, H.-Ho Lee, J.-M. Kwon, M. Choi, B.-Ho Park, J.-Gu Kwak, W.-C. Kim, Y.-Un Nam, S. Wang, J.-H. Jeong, K.-R. Park, Y.-S. Kim, Y. In, H. K. Park, G. Yun, W. Choe, Y.-C. Ghim, Y.-S. Na, and Y.-S. Hwang. Progress of the kstar research program exploring the advanced high performance and steady-state plasma operations. *Journal of the Korean Physical Society*, 73:1–24, 2018.

[31]L. R. Baylor, T. C. Jernigan, S. K. Combs, W. A. Houlberg, M. Murakami, P. Gohil, K. H. Burrell, C. M. Greenfield, R. J. Groebner, C.-L. Hsieh, R. J. La Haye, P. B. Parks, G. M. Staebler, DIII-D Team, G. L. Schmidt, D. R. Ernst, E. J. Synakowski, and M. Porkolab. Improved core fueling with high field side pellet injection in the diii-d tokamak. *Phys. Plasmas*, 7(1878), 2000.

[32]F. Jenko, W. Dorland, M. Kotschenreuther, and B. N. Rogers. Electron temperature gradient driven turbulence. *Phys. Plasmas*, 7(1904), 2000.

[33]M. A. Van Zeeland, R. L. Boivin, T. N. Carlstrom, T. Deterly, and D. K. Finkenthal. Fiber optic two-color vibration compensated interferometer for plasma density measurements. *Rev. Sci. Instrum*, 77(10F325), 2006.

[34]D. M. Ponce-Marquez, B. D. Bray, T. M. Deterly, C. Liu, and D. Eldon. Thomson scattering diagnostic upgrade on diii-d. *Rev. Sci. Instrum.*, 81(10D525), 2010.

[35]K. H. Burrell, P. Gohil, R. J. Groebner, D. H. Kaplan, J. I. Robinson, and W. M. Solomon. Improved charge-coupled device detectors for high-speed, charge exchange spectroscopy studies on the diii-d tokamak. *Rev. Sci. Instrum*, 75(10):3455, 2004.

[36]M. E. Austin and J. Lohr. Electron cyclotron emission radiometer upgrade on the diii-d tokamak. *Rev. Sci. Instrum.*, 74:1457, 2003.

[37]Y. Wang, B. Tobias, Y.-T. Chang, J.-H. Yu, M. Li, F. Hu, M. Chen, M. Mamidanna, T. Phan, A.-V. Pham, J. Gu, X. Liu, Y. Zhu, C.W. Domier, L. Shi, E. Valeo, G.J. Kramer, D. Kuwahara, Y. Nagayama, A. Mase, , and N.C. Luhmann Jr. Millimeter-wave imaging of magnetic fusion plasmas: technology innovations advancing physics understanding. *Nucl. Fusion*, 57(5):072007, 2017.

[38]L. Bardóczi, T. L. Rhodes, T. A. Carter, A. Bañón Navarro R. J. La Haye, and G. R. McKee. Shrinking of core neoclassical tearing mode magnetic islands due to edge localized modes and the role of ion-scale turbulence in island recovery in diii-d. *Phys. Plasmas*, 24(062503), 2017.

[39]J. D. King, R. J. La Haye, C. C. Petty, T. H. Osborne, C. J. Lasnier, R. J. Groebner, F. A. Volpe, M. J. Lanctot, M. A. Makowski, C. T. Holcomb, W. M. Solomon, S. L. Allen, T. C. Luce, M. E. Austin, W. H. Meyer, and E. C. Morse. Hybrid-like 2/1 flux-pumping and magnetic island evolution due to edge localized mode-neoclassical tearing mode coupling in diii-d. *Phys. Plasmas*, 19(022503), 2012.

[40]L. Bardóczi, T. L. Rhodes, A. Bañón Navarro, C. Sung, T. A. Carter, R. J. La Haye, C. Petty, C. Crystal, and F. Jenko. Impact of neoclassical tearing mode - turbulence multi-scale interaction in confinement degradation and magnetic island stability. *Phys. Plasmas*, 24(122503), 2017.

[41]L. Bardóczi, M. Podestà, W. W. Heidbrink, and M. A. Van Zeeland. Quantitative modeling of neoclassical tearing mode driven fast ion transport in integrated transp simulations. *Plasma Phys. Control. Fusion*, (submitted), 2009.

[42]Snyder P B, Wilson H R, Ferron J R, Lao L L, Leonard A W, Osborne T H, Turnbull A D, Mossessian D, Murakami M, and Xu X Q. Edge localized modes and the pedestal: A model based on coupled peeling-ballooning modes. *Phys. Plasmas*, 9:2037–43, 2002.

[43]M. Knolker, A. Bortolon, G.P. Canal, T.E. Evans, H. Zohm, T. Abrams, R.J. Buttery, E.M. Davis, R.J. Groebner, and E. Hollmann. Investigation of the role of pedestal pressure and collisionality on type-i elm divertor heat loads in diii-d. *Nucl. Fusion*, 58(096023), 2018.

[44]D. Wróblewski and L. L. Lao. Polarimetry of motional stark effect and determination of current profiles in diiid (invited). *Rev. Sci. Instrum.*, 63(5140), 1992.

[45]R. J. Buttery, R. J. La Haye, P. Gohil, G. L. Jackson, H. Reimerdes, E. J. Strait, and the DIII-D Team. The influence of rotation on the β threshold for the 2/1 neoclassical tearing mode in diii-d. *Phys. Plasmas*, 15(056115), 2008.

[46]D. A. Gates and L. Delgado-Aparicio. Origin of tokamak density limit scalings. *Phys. Rev. Lett.*, 108(165004), 2012.

[47]P. Maget, F. Widmer, O. Février, X. Garbet, and H. Lutjens. Stabilization of a magnetic island by localized heating in a tokamak with stiff temperature profile. *Phys. Plasmas*, 25(022514), 2018.

[48]A. H. Reiman and N. J. Fish. Suppression of tearing modes by radio frequency current condensation. *Phys. Rev. Lett.*, 121(225001), 2018.

[49]G. R. McKee, R. J. Fonck, M. W. Shafer, I. U. Uzun-Kaymak, and Z. Yan. Wide-field turbulence imaging with beam emission spectroscopy. *Rev. Sci. Instrum.*, 81(10D741), 2010.

[50]A. Bañón Navarro, L. Bardóczi, T. A. Carter, F. Jenko, and T. L. Rhodes. Effect of magnetic islands on profiles, flows, turbulence and transport in nonlinear gyrokinetic simulations. *Plasma Physics and Controlled Fusion*, 59(3):034004, 2017.

[51]A. M. Dimits, G. Bateman, M. A. Beer, B. I. Cohen, W. Dorland, G. W. Hammett, C. Kim, J. E. Kinsey, M. Kotschenreuther, A. H. Kritz, L. L. Lao, J. Mandrekas, W. M. Nevins, S. E. Parker, A. J. Redd, D. E. Shumaker, R. Sydora, and J. Weiland. Comparisons and physics basis of tokamak transport models and turbulence simulations. *Phys. Plasmas*, 7(969), 2000.

[52]W. A. Hornsby, A. G. Peeters, A. P. Snodin, F. J. Casson, Y. Camenen, G. Szepesi, M. Siccinio, and E. Poli. The nonlinear coupling between gyroradius scale turbulence and mesoscale magnetic islands in fusion plasmas. *Phys. Plasmas*, 17(092301), 2010.

[53]D. Zarzoso, W.A. Hornsby, E. Poli, F.J. Casson, and A.G. Peeterssand S. Nasr. Impact of rotating magnetic islands on density profile flattening and turbulent transport. *Nucl. Fusion*, 55(113018), 2015.